Particle-in-cell simulation of laser wakefield accelerators with oblique lasers in quasicylindrical geometry

Minghao Ma,[1] Ming Zeng,[2,3,*] Jia Wang,[2,3] Guangwei Lu,[1] Wenchao Yan,[1,4,†] Liming Chen,[1,4] and Dazhang Li[2,3]

[1]*Key Laboratory of Laser Plasma (MoE), School of Physics and Astronomy, Shanghai Jiao Tong University, Shanghai 200240, China*
[2]*Institute of High Energy Physics, Chinese Academy of Sciences, Beijing 100049, China*
[3]*University of Chinese Academy of Sciences, Beijing 100049, China*
[4]*IFSA Collaborative Innovation Center, Shanghai Jiao Tong University, Shanghai 200240, China*

(Received 20 April 2024; accepted 15 January 2025; published 7 February 2025)

In the studies of optical injections in laser or beam-driven wakefield accelerators, there is a frequent demand for using obliquely propagating assistant lasers in particle-in-cell simulations. In conventional methods, this is only possible in either two- or three-dimensional Cartesian geometries, which have the drawbacks of either lack of fidelity for the actual situation or requiring a huge amount of computational resources. In this work, we develop a new method that uses an expression-defined oblique laser field to simulate such situations in quasicylindrical geometry particle-in-cell simulations, having the advantages of both maintaining good fidelity and saving computational resources. As an example, we use this method in the scissor-cross ionization injection scheme for the optimization of the injected beam quality. This method is widely applicable to particle injections with assistant lasers in wakefield accelerators, as long as the assistant lasers only influence the injected particles during the injection process.

DOI: 10.1103/PhysRevAccelBeams.28.021301

I. INTRODUCTION

Laser wakefield accelerator (LWFA) has received much attention since it was proposed due to its high acceleration gradient [1]. In 2004, quasimonoenergetic electron beams were obtained experimentally from LWFAs for the first time [2–4]. In the following two decades, scientists have been continuously improving the quality and reliability of LWFAs for real applications [5,6]. The quality of the accelerated electron beam in an LWFA mainly depends on the injection scheme. The commonly used schemes include self-injection [7–10], injection by modulation of phase velocity of plasma wake [11–17], ionization injection [18–30], and injection by laser collision [31–34]. Scissor-cross ionization injection is an improvement of the ionization injection scheme, which uses an oblique assistant laser to intersect with the driving laser at an acute angle, and thus triggers the ionization injection when the two lasers overlap [35].

Particle-in-cell (PIC) algorithm is a widely used simulation method for laser-plasma interactions and is one of the most important tools in LWFA studies. The PIC algorithm in three-dimensional (3D) geometry is usually considered to have the most fidelity to the real situation, at the cost of huge consumption of computational resources. Recently, the analytic pulse technique (APT) for computational electromagnetics has been proposed to reduce the computational cost [36]. The APT optimizes the PIC loop by decomposing electromagnetic fields into analytically solved vacuum fields and numerically solved plasma response fields. Besides, the quasicylindrical geometry (QCG) is developed for PIC simulations to save computational resources while maintaining fidelity for the problems with partial cylindrical symmetry [37–40]. In such a problem, the system can be decomposed into a finite number of azimuthal modes, so that the original 3D problem is reduced to a few two-dimensional problems, and the time and space complexities are largely reduced. The LWFA with a cylindrically symmetric laser profile is a very typical problem suitable for the QCG. Thus, PIC with QCG is becoming one of the most commonly used methods for LWFA simulations. However, for problems without such partial cylindrical symmetry, such as problems involving transverse or oblique assistant lasers, the QCG is usually not applicable.

In this paper, we propose to use an expression-defined laser field in the QCG to simulate the LWFA problems with

*Contact author: zengming@ihep.ac.cn
†Contact author: wenchaoyan@sjtu.edu.cn

oblique lasers, as suggested in a private discussion [41]. In this method, the driving laser is conventionally launched on the simulation grids and propagates self-consistently in the longitudinal direction, while the oblique laser is defined by math expressions of electromagnetic (EM) field. Similar to APT, the oblique laser is prescribed, but we apply it to the QCG, and the particle response is realized in the species ionization and particle pushing processes of the PIC cycle. In practice, such an expression-defined field is realizable by the "external EM field" feature in most PIC codes [42]. However, the validity of using such an external oblique laser field in the QCG, which is far away from cylindrical symmetry, has not been proved before. Three simulation tests of this method are in Sec. II, the application of this method to the scissor-cross ionization injection scheme is in Sec. III, and Sec. IV concludes this paper. We demonstrate that although the oblique laser breaks the symmetry, the QCG simulation can still maintain a satisfactory fidelity compared with 3D simulations in the Cartesian geometry. As one can see, this method makes the parameter scan of LWFAs with oblique assistant lasers possible, which is usually unaffordable in the conventional 3D Cartesian geometry.

II. SIMULATION TESTS OF OBLIQUE LASERS IN THE QUASICYLINDRICAL GEOMETRY

In our method, the driving laser is linearly polarized and has a cylindrically symmetric spatial profile, and it is launched by the regular laser launching mechanism of a PIC code. The self-consistent evolution of such a laser can be simulated with high fidelity in the QCG. The assistant laser coming from the side, usually at an oblique angle, is realized by defining the expressions of its EM field. To find the expressions, we first write down the vector potential of the laser in its self-coordinate (x', y', z'), where $z'+$ is the propagation direction, and x' is the polarization direction of the laser. If we assume the laser profile is Gaussian both temporally and spatially, and the interaction region is much shorter than the Rayleigh length, the vector potential (normalized to $m_e c/e$, where m_e is the electron mass, c is the speed of light in vacuum, and e is the elementary charge) near the focal position can be written as

$$A_{x'} = a_0 \cos(kz' - \omega t) \exp\left[-\frac{r'^2}{w_0^2} - \frac{(\frac{z'}{c} - t)^2}{\tau^2}\right], \quad (1)$$

and $A_{y'} = A_{z'} = 0$, where a_0 is the amplitude of the normalized vector potential, ω is the laser angular frequency, $k = \omega/c$ is the laser wave number, w_0 is the focal radius, τ is the pulse duration, and $r' = \sqrt{x'^2 + y'^2}$ is the transverse position. Within the focal region determined by the Rayleigh length $z_R = kw_0^2/2$, the laser radius does not change significantly so that the simplified expression Eq. (1) can be applied. Then, the expressions of the laser EM field can be obtained based on $E_{x'} = -\partial A_{x'}/\partial t$, $B_{y'} = \partial A_{x'}/\partial z'$, and $B_{z'} = -\partial A_{x'}/\partial y'$. Finally, the expressions of (E_x, E_y, E_z) and (B_x, B_y, B_z) in the simulation coordinate (x, y, z) are obtained by rotation of coordinates. This method can be applied as long as the evolution of the assistant laser can be expressed by functions of t and (x, y, z). This EM field is directly applied to the electron pushing and the species ionization algorithms, without being solved by the EM field solver.

Generally, the assistant laser passes through a shorter plasma region, and its power is smaller compared with the driving laser. These lead to a less significant laser-plasma interaction for the assistant laser, such as the self-focusing effect. In this case, the evolution of the assistant laser can be approximated as vacuum propagation, because the plasma only makes very slight changes to the parameters of the assistant laser. If more accurate assistant laser parameters are required, such as the focal spot size and intensity modified by the self-focusing effect, they can be estimated theoretically or obtained through another PIC simulation.

In the following, we test our method in three very simple cases using the code WarpX with the pseudospectral analytical time domain solver [43–47]. We use a very dilute uniform plasma satisfying $a_0/(k_p w_0)^2 \gtrsim 1$, where $k_p = \sqrt{4\pi r_e n_p}$ is the wave number of the plasma wake, r_e is the classical electron radius, and n_p is the unperturbed plasma density. This condition implies that the EM field from the plasma is negligible compared with the laser field [48], which is beneficial for the testing of the particle scattering in the laser field [49]. In practice, we set $a_0 = 2$, $k/k_p = 4.2 \times 10^8$, $kw_0 = 39.3$, and $\omega\tau = 47.1$ in the tests of this section. The QCG is used with 4 azimuthal modes, and 32 macroparticles per cell in total (8 in the azimuthal direction, 2 in the longitudinal direction, and 2 in the radial direction). The transverse cell size is $dr = \lambda/4$, the longitudinal cell size is $dz = \lambda/33$, where λ is the laser wavelength, and the time step is dz/c. For comparison, simulations in 3D Cartesian geometry have also been performed with the Cole-Karkkainen solver [50].

A. Electron scattering by a single oblique laser

We add a single oblique laser using the method above. The scattering of electrons by such a laser with the aforementioned parameters and $\theta = 45°$ oblique angle is tested, as shown in Fig. 1. Plasma electrons are pushed outward due to the ponderomotive effect [51], creating a plasma channel, as shown in Fig. 1(a). We also see a density perturbation in the symmetric direction (from up left to down right), which is nonphysical due to the imperfections of the QCG to this problem. As a comparison, the simulation in the 3D Cartesian geometry with the same parameters is shown in Fig. 1(b), which does not have such a nonphysical effect. Nevertheless, such imperfections do not impact the momentum that electrons obtained from the

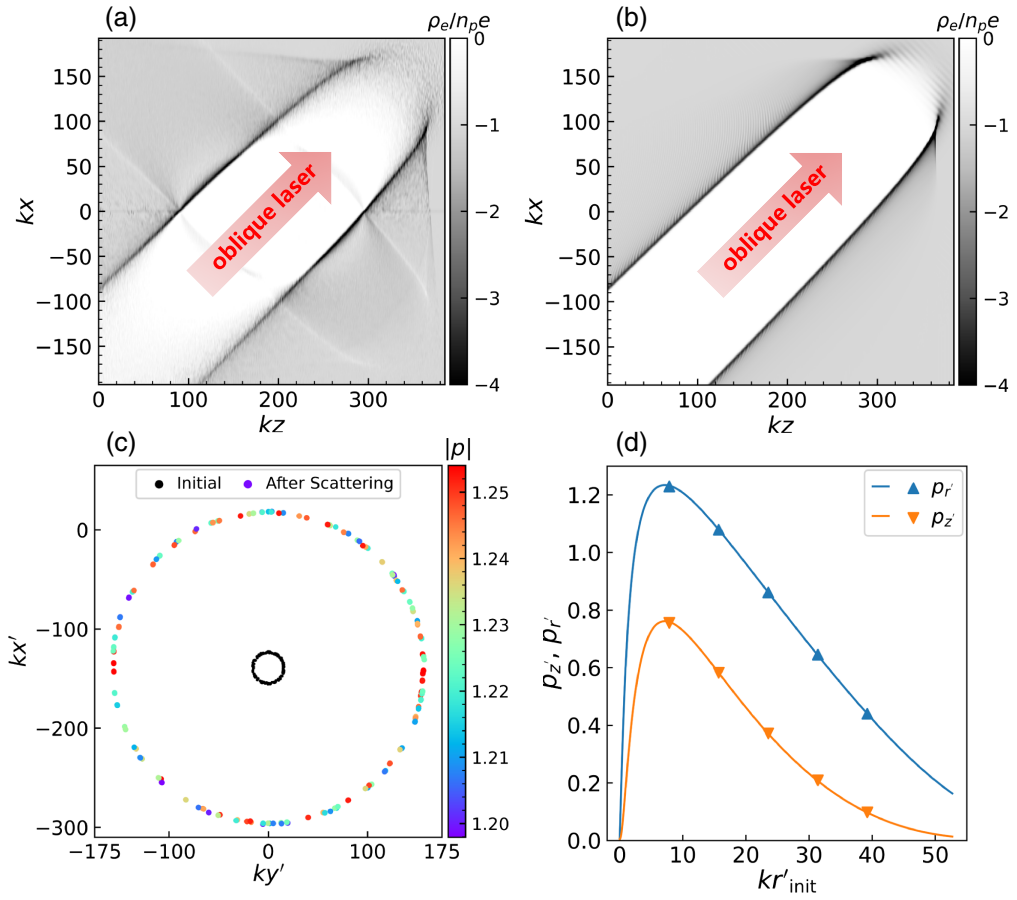

FIG. 1. A PIC simulation test of electrons scattered by a single oblique laser. (a) Electron charge density distribution ρ_e in the QCG after the laser comes into the plasma from bottom left to up right. The shadow from up left to bottom right is a minor nonphysical effect due to the imperfect representation of the plasma response to the oblique laser in the QCG. (b) The simulation plot in the 3D Cartesian geometry with the same parameters as (a). (c) Distribution of position and momentum of some sample electrons at two different time steps in the laser's self-coordinate (x', y') from the QCG simulation. Black dots: initial positions of electrons before laser comes; colored dots: positions of the electrons after being scattered by the laser. The color reflects the amplitude of the momentum $|p|$, which is normalized to $m_e c$. (d) The final momentum (normalized to $m_e c$) in z' and r' directions vs the initial position r'_{init} for the electrons scattered by the laser. The triangles are obtained by the PIC simulation in the QCG, while the solid lines are obtained by the numerical solutions of a particle tracking code [52].

scattering in the QCG, as shown in Figs. 1(c) and 1(d). In Fig. 1(c), we see that the electrons with similar initial positions $kr'_{\text{init}} = 7.85 \pm 0.39$ form a circle after the scattering, because their velocities have almost the same amplitude but different directions. The difference in their final momentum is due to the slight difference in r'_{init}. We have also verified the final momentum distribution using a particle tracking code, which numerically solves the electron trajectories under the influence of the laser field [52], as shown in Fig. 1(d). One can see that the results from the PIC simulation almost perfectly match the particle tracking solution.

B. Electron scattering by two lasers

Now we add a longitudinally propagating laser, called the driving laser, using the regular laser launching mechanism of WarpX. The oblique laser, called the colliding laser, is just the same as in Sec. II A. The parameters of the two lasers are the same, except for their propagation directions. The two lasers cross inside the simulation region, which is filled with the uniform dilute plasma, as shown in Figs. 2(a)–2(c). The plasma electrons undergo a stochastic acceleration, which means two electrons with slightly different initial positions can have very different trajectories after the scattering [53,54]. Thus, precise tracking of the scattered electrons is impossible. Nevertheless, a statistical prediction of them is possible. We show the final momentum distribution of the electrons, which are initially located within a small cylinder $157 < kz < 236$ and $kr < 39$, where $r = \sqrt{x^2 + y^2}$, in Figs. 2(d)–2(f). In order to verify our method, we have also performed the same simulation in the 3D Cartesian geometry, which has almost the same results as the QCG simulation, as one can see in Figs. 2(d)–2(f).

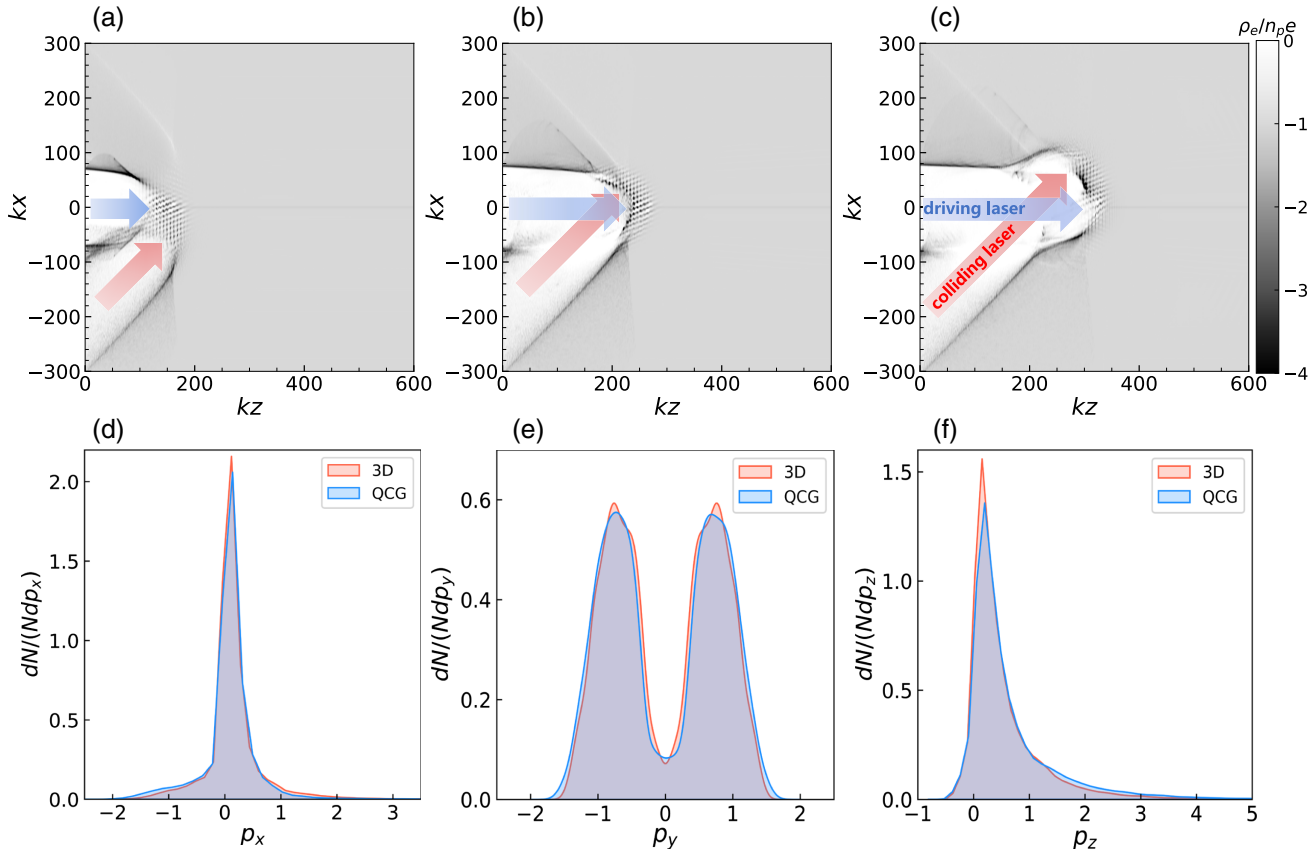

FIG. 2. The PIC simulation test of our method of electron scattering by two lasers. (a–c) The plasma electron density distribution during the collision of the two lasers in the QCG. (d–f) The comparison of the distribution of electron momentum p_x, p_y, and p_z (normalized to $m_e c$) after being fully scattered by the two lasers in the 3D Cartesian geometry and the QCG.

C. Ionization ratio of N^{5+} by two lasers

Nitrogen is commonly used for the ionization injection of LWFAs. For a nitrogen atom, the outer shell electrons are usually ionized at a very early stage of the laser pulse due to their relatively low ionization threshold, and the ion N^{5+} is usually remained for the ionization injection, which has the ionization threshold of $a_0 \sim 2$ for the laser with the wavelength of $\lambda = 0.8$ μm.

In this test, we use the same two lasers as in Sec. II B and $\lambda = 0.8$ μm, but the plasma is replaced by a uniform N^{5+} region located within $157 < kz < 236$ and $kr < 39$. As the simulation starts, N^{5+} is gradually ionized to N^{6+} or N^{7+} due to the electric field of the two lasers. The evolution of ionization ratio, defined as the number of released electrons divided by the initial number of N^{5+}, is plotted for both QCG and 3D Cartesian geometry simulations in Fig. 3. We have varied a_0 from 1.8 to 2.1 to compare the results in both geometries and find that the ionization ratio in the QCG is slightly (up to 4%) smaller than in the 3D Cartesian geometry. Such difference is due to the slightly (~1%) different superimposed electric field strengths in the two geometries, as the ionization ratio is very sensitive to the field strength when it is near the ionization threshold of N^{5+}. We have also performed a series of convergence tests with smaller cell sizes (dz, dr) and increased number of macroparticles per cell and found that the ionization ratio difference can be reduced by decreasing either dz or dr.

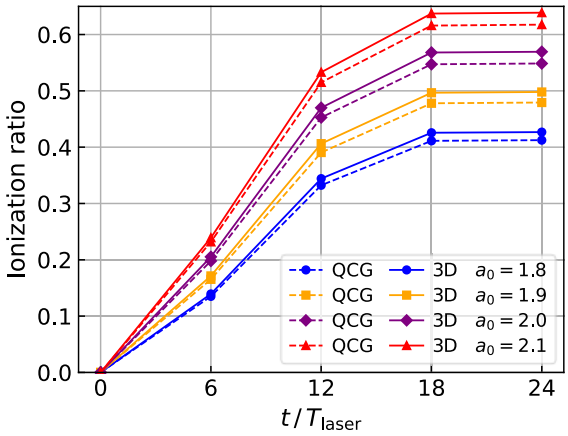

FIG. 3. The ionization ratio of the N^{5+} ion vs time (normalized to laser cycle T_{laser}) obtained in both QCG and 3D Cartesian geometry simulations. Four cases of a_0 are tested, and in each of the cases, a_0 is the same for both the driving and colliding lasers.

Specifically, when dz is reduced to $\lambda/66$ for the $a_0 = 1.8$ case, the ionization ratio increases by 1.5% in the QCG and by 0.8% in the 3D case. We use $dz = \lambda/33$ as a good trade-off between accuracy and cost.

III. SIMULATION OF SCISSOR-CROSS IONIZATION INJECTION IN THE QUASICYLINDRICAL GEOMETRY

In the ionization injection, the main problem is that the injection process is usually continuous, which leads to a large energy spread of the produced beam. By using the self-truncated ionization injection scheme, the minimal energy spread can reach ∼5% [26,28,29]. By controlling the charge through localized ionization injection to optimize the beam loading, ∼1% energy spread can be obtained [30]. Recently, another improved ionization injection scheme, called the scissor-cross ionization injection, has been proposed, which produces electron beams down to 1%–2% energy spread. In this injection scheme, an oblique assistant laser intersects with the driving laser at an acute angle θ, and the ionization of the inner shell of the atom is only possible when the two lasers overlap [35]. Thus, the length of the injection region and consequently the energy spread of the produced beam are controllable by adjusting the crossing angle θ. In conventional methods, the simulation of the scissor-cross ionization injection is only possible in either 2D (two-dimensional) or 3D Cartesian geometries. While the parameter scan is unaffordable in 3D, the 2D simulations usually do not represent the real situation well. Especially in the cases where the transverse size of the driving laser evolves significantly, the energy conservation in the 2D geometry leads to the constant of a^2w, where a and w are the instant values of the vector potential amplitude and the transverse size of the laser, respectively. In real situation, however, a^2w^2 should be a constant, instead.

A high-fidelity parameter scan of the scissor-cross ionization injection is possible using the method proposed in this paper. We redo a similar simulation as in Ref. [35], using the QCG and the expression-defined oblique laser field. Because the interaction time between the two lasers is short and the injected electrons do not interact with the oblique laser anymore after the injection, the nonphysical effects due to the breaking of the cylindrical symmetry, such as the nonphysical shadow in Fig. 1(a), are not conveyed by the electron beam in the long acceleration process.

In the simulation, the driving laser has $a_0 = 2.74$, $\lambda = 0.8$ μm, $w_0 = 20$ μm, and $\tau = 30$ fs, while the oblique laser has $a_0 = 1.37$, $\lambda = 0.4$ μm, $w_0 = 20$ μm, and $\tau = 30$ fs. Both lasers are polarized in the y direction, while they propagate in the $x - z$ plane. The plasma is preionized with a linear up-ramp from $z = -30$ to 0 μm and a plateau with the density $n_p = 1.36 \times 10^{18}$ cm^{-3} from $z = 0$ to $+\infty$. The simulation cell size is $dz = 0.0234$ μm, $dr = 0.234$ μm, the time step is $dt = dz/c$, the number of azimuthal modes is 4, and the macroparticle number per cell is 32 (8 in the azimuthal direction). The preionized species is Ne^{8+} with the density of $n_p/8$, which means the plasma is provided by the preionization of the outer-shell electrons of the neutral Ne gas. Because the ionization threshold of Ne^{8+} is $a_0 \sim 4$ for the laser with $\lambda = 0.8$ μm, it is guaranteed that any further ionization of Ne^{8+} is impossible by the driving laser only, even if the intensity of the driving laser is slightly increased due to the self-focusing effect. The oblique laser intersects with the driving laser at $z = 40$ μm and the crossing angle θ to assist the further ionization of Ne^{8+}.

We first check the phase space distribution of the injected beam shortly after the injection occurs for the $\theta = 8°$ case, as shown in Fig. 4(a). As a comparison, we also show the same plot from a 3D Cartesian geometry simulation with the same configuration in Fig. 4(b). One can see that the injected beams in these two simulations are similar, though the mean energy is slightly lower in the 3D case (18 MeV in the QCG, and 17 MeV in the 3D case). The difference is probably due to the beam loading effect of the different beam charge, which is 66 pC in the QCG and 73 pC in the 3D case. When the two lasers overlap, the maximum superimposed electric field in the 3D is slightly (up to ∼1.5%) higher than in the QCG, which causes the ∼10% difference in the injected charge. Such an enlarged difference is because the ionization ratio is sensitive to the electric field strength if the field strength is near the ionization threshold. Nevertheless, since even a 3D simulation cannot perfectly reflect the real situation due to such sensitivity, we regard this difference to be acceptable.

Next, we apply our method to the scan of the crossing angle θ from 8° to 30°. For different θ, the two lasers overlap for a different duration, so the charge of the beam from the ionization injection is different. The acceleration process afterward is not affected by the oblique laser, but the beam quality is influenced by the status of the injection. For each θ case, the injected beam is accelerated and undergoes a phase space rotation process. Thus, the energy increases, and the energy spread decreases initially. After a certain length, the energy spread is minimal and starts to increase. This length is the optimal acceleration length L_{opt}. Each of the simulations is performed to exceed L_{opt}, and the evolution of the energy spread is shown in Fig. 4(c). One can see that L_{opt} increases as θ increases. Moreover, there is a minimal energy spread for all cases at $\theta = 20°$ as shown in Fig. 4(d). We also plot the beam charge from the ionization injection Q_i and from the background plasma Q_b in Fig. 4(d) and see that Q_i decreases, while Q_b increases, with an increasing θ. For a smaller θ, the overlapping region of the two lasers (which is approximately the injection region) is long, thus Q_i is more and

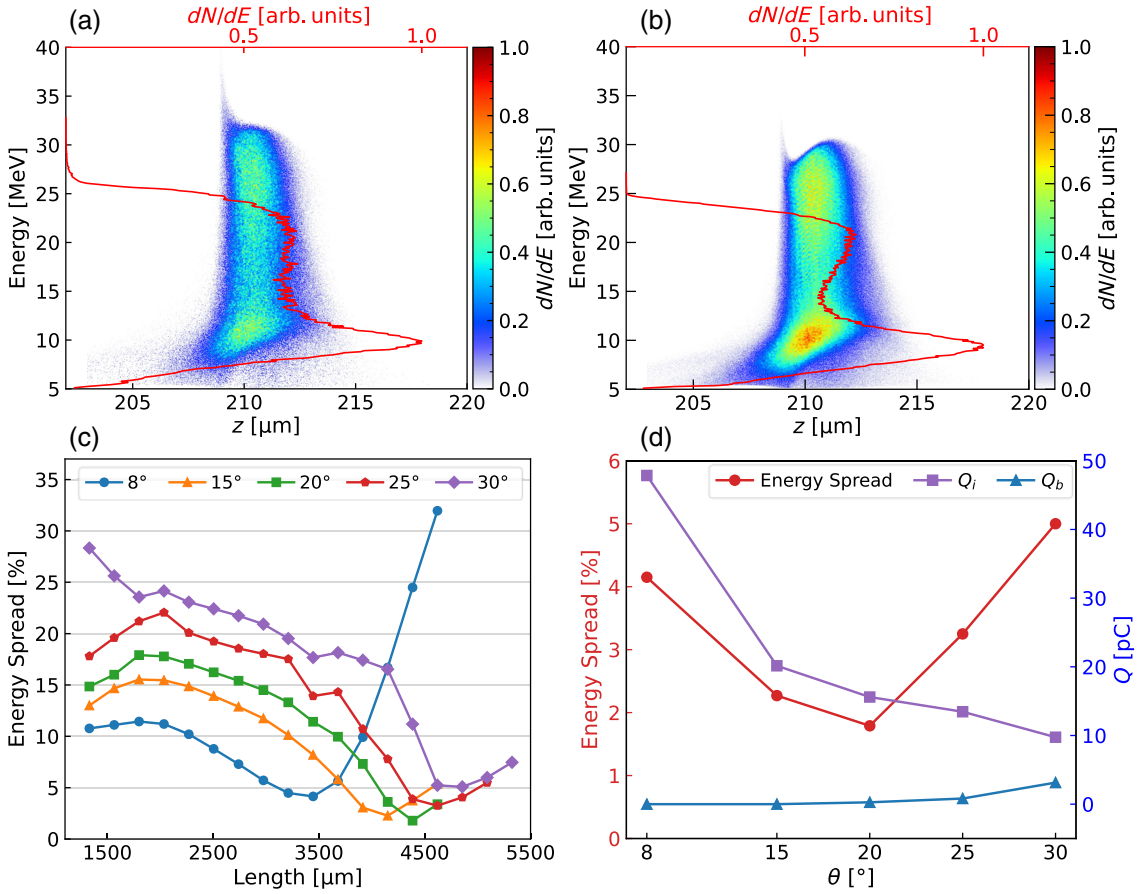

FIG. 4. The PIC simulation results for the LWFA with the scissor-cross ionization injection. (a) The phase space distribution of the injected electrons shortly after the crossing of the two lasers occurs in a QCG simulation. The red line shows the energy spectrum. The crossing angle of the two lasers is $\theta = 8°$. (b) The same simulation, but in the 3D Cartesian geometry. (c) The energy spread of the injected beam vs acceleration length for different θ, obtained by the simulations in QCG. (d) The minimum energy spread during the acceleration for each of the θ cases. The charge numbers from the inner-shell ionization Q_i and from the background plasma Q_b are also plotted.

the energy spread is relatively larger. The beam is purely from ionization injection for a small θ, as Q_b is negligible for $\theta < 25°$. For a larger θ, the overlapping region of the two lasers is short, thus causing Q_i to decrease. However, the injection mechanism is gradually transformed into the laser collision injection of the background plasma electrons, as Q_b increases and becomes significant for $\theta > 25°$. In the cases with coexisting ionization injection and laser collision injection, the electrons are spread in different regions of the phase space, which cannot form a beam with very low energy spread. Thus, the minimal energy spread is achieved for a moderate crossing angle of $\theta = 20°$, with a relatively short injection length and a negligible Q_b. The optimal case at $\theta = 20°$ has the beam with a charge of 16 pC, an energy of 510 MeV, and an energy spread of 1.8%, and we show the whole acceleration process in Supplemental Material [55]. One may notice that the optimal $\theta = 20°$ is different from the original paper of this injection mechanism, which has the optimal at $\theta = 30°$, because the scan was performed in the 2D Cartesian geometry in the original paper [35].

IV. CONCLUSION

In this paper, we propose to use an expression-defined EM field to simulate the LWFA problems with oblique lasers in PIC codes with the quasicylindrical geometry, in order to reduce the simulation costs while maintaining the fidelity. This method has been tested in three simple cases and applied to the scissor-cross ionization injection for the scanning of the optimal crossing angle. We demonstrate that although the oblique laser breaks the symmetry, the QCG can still obtain the results with high fidelity. This method is widely applicable to problems with the EM field, which breaks the cylindrical symmetry as long as the evolution of the EM field is predictable by expressions, and the interaction time of the EM field with the plasma is short. Especially, it can also be applied to the beam-driven plasma wakefield accelerators with oblique assistant lasers [49,56].

ACKNOWLEDGMENTS

M. Z. acknowledges Jean-Luc Vay for an original idea of the method proposed in this work. This work is supported

by the Strategic Priority Research Program of the Chinese Academy of Sciences (Grant No. XDB0530000), the National Key Programme for S&T Research and Development of China (2021YFA1601700), and the National Natural Science Foundation of China (12074251, 11991073, and 12475159). We thank the sponsorship from Yangyang Development Fund. This research used the open-source particle-in-cell code WarpX [57], primarily funded by the U.S. DOE Exascale Computing Project. Primary WarpX contributors are with LBNL, LLNL, CEA-LIDYL, SLAC, DESY, CERN, and TAE Technologies. We acknowledge all WarpX contributors.

[1] T. Tajima and J. M. Dawson, Laser electron accelerator, Phys. Rev. Lett. **43**, 267 (1979).

[2] C. G. R. Geddes, C. Toth, J. van Tilborg, E. Esarey, C. B. Schroeder, D. Bruhwiler, C. Nieter, J. Cary, and W. P. Leemans, High-quality electron beams from a laser wakefield accelerator using plasma-channel guiding, Nature (London) **431**, 538 (2004).

[3] S. P. D. Mangles, C. D. Murphy, Z. Najmudin, A. G. R. Thomas, J. L. Collier, A. E. Dangor, E. J. Divall, P. S. Foster, J. G. Gallacher, C. J. Hooker, D. A. Jaroszynski, A. J. Langley, W. B. Mori, P. A. Norreys, F. S. Tsung, R. Viskup, B. R. Walton, and K. Krushelnick, Monoenergetic beams of relativistic electrons from intense laser-plasma interactions, Nature (London) **431**, 535 (2004).

[4] J. Faure, Y. Glinec, A. Pukhov, S. Kiselev, S. Gordienko, E. Lefebvre, J.-P. Rousseau, F. Burgy, and V. Malka, A laser-plasma accelerator producing monoenergetic electron beams, Nature (London) **431**, 541 (2004).

[5] A. J. Gonsalves *et al.*, Petawatt laser guiding and electron beam acceleration to 8 GeV in a laser-heated capillary discharge waveguide, Phys. Rev. Lett. **122**, 084801 (2019).

[6] A. R. Maier, N. M. Delbos, T. Eichner, L. Hübner, S. Jalas, L. Jeppe, S. W. Jolly, M. Kirchen, V. Leroux, P. Messner, M. Schnepp, M. Trunk, P. A. Walker, C. Werle, and P. Winkler, Decoding sources of energy variability in a laser-plasma accelerator, Phys. Rev. X **10**, 031039 (2020).

[7] A. Modena, Z. Najmudin, A. Dangor, C. Clayton, K. Marsh, C. Joshi, V. Malka, C. Darrow, C. Danson, D. Neely, and F. Walsh, Electron acceleration from the breaking of relativistic plasma waves, Nature (London) **377**, 606 (1995).

[8] C. B. Schroeder, E. Esarey, and B. A. Shadwick, Warm wave breaking of nonlinear plasma waves with arbitrary phase velocities, Phys. Rev. E **72**, 055401 (2005).

[9] S. Y. Kalmykov, L. M. Gorbunov, P. Mora, and G. Shvets, Injection, trapping, and acceleration of electrons in a three-dimensional nonlinear laser wakefield, Phys. Plasmas **13**, 113102 (2006).

[10] W. Yan, L. Chen, D. Li, L. Zhang, N. A. M. Hafz, J. Dunn, Y. Ma, K. Huang, L. Su, M. Chen, Z. Sheng, and J. Zhang, Concurrence of monoenergetic electron beams and bright x-rays from an evolving laser-plasma bubble, Proc. Natl. Acad. Sci. U.S.A. **111**, 5825 (2014).

[11] S. Bulanov, N. Naumova, F. Pegoraro, and J. Sakai, Particle injection into the wave acceleration phase due to nonlinear wake wave breaking, Phys. Rev. E **58**, R5257 (1998).

[12] A. V. Brantov, T. Z. Esirkepov, M. Kando, H. Kotaki, V. Y. Bychenkov, and S. V. Bulanov, Controlled electron injection into the wake wave using plasma density inhomogeneity, Phys. Plasmas **15**, 073111 (2008).

[13] C. G. R. Geddes, K. Nakamura, G. R. Plateau, C. Toth, E. Cormier-Michel, E. Esarey, C. B. Schroeder, J. R. Cary, and W. P. Leemans, Plasma-density-gradient injection of low absolute-momentum-spread electron bunches, Phys. Rev. Lett. **100**, 215004 (2008).

[14] F. Li, T. N. Dalichaouch, J. R. Pierce, X. Xu, F. S. Tsung, W. Lu, C. Joshi, and W. B. Mori, Ultrabright electron bunch injection in a plasma wakefield driven by a superluminal flying focus electron beam, Phys. Rev. Lett. **128**, 174803 (2022).

[15] J. Wang, M. Zeng, D. Li, X. Wang, W. Lu, and J. Gao, Injection induced by coaxial laser interference in laser wakefield accelerators, Matter Radiat. Extremes **7**, 054001 (2022).

[16] J. Wang, M. Zeng, D. Li, X. Wang, and J. Gao, High quality beam produced by tightly focused laser driven wakefield accelerators, Phys. Rev. Accel. Beams **26**, 091303 (2023).

[17] X. Xu, T. N. Dalichaouch, J. Liu, Q. Ma, J. Pierce, K. Miller, X. Yan, and W. B. Mori, Generation of ultrabright and low energy spread electron beams in laser wakefield acceleration in a uniform plasma, Phys. Rev. Accel. Beams **26**, 111302 (2023).

[18] M. Chen, Z.-M. Sheng, Y.-Y. Ma, and J. Zhang, Electron injection and trapping in a laser wakefield by field ionization to high-charge states of gases, J. Appl. Phys. **99**, 056109 (2006).

[19] E. Oz *et al.*, Ionization-induced electron trapping in ultrarelativistic plasma wakes, Phys. Rev. Lett. **98**, 084801 (2007).

[20] C. McGuffey, A. G. R. Thomas, W. Schumaker, T. Matsuoka, V. Chvykov, F. J. Dollar, G. Kalintchenko, V. Yanovsky, A. Maksimchuk, K. Krushelnick, V. Y. Bychenkov, I. V. Glazyrin, and A. V. Karpeev, Ionization induced trapping in a laser wakefield accelerator, Phys. Rev. Lett. **104**, 025004 (2010).

[21] A. Pak, K. A. Marsh, S. F. Martins, W. Lu, W. B. Mori, and C. Joshi, Injection and trapping of tunnel-ionized electrons into laser-produced wakes, Phys. Rev. Lett. **104**, 025003 (2010).

[22] C. E. Clayton, J. E. Ralph, F. Albert, R. A. Fonseca, S. H. Glenzer, C. Joshi, W. Lu, K. A. Marsh, S. F. Martins, W. B. Mori, A. Pak, F. S. Tsung, B. B. Pollock, J. S. Ross, L. O. Silva, and D. H. Froula, Self-guided laser wakefield acceleration beyond 1 GeV using ionization-induced injection, Phys. Rev. Lett. **105**, 105003 (2010).

[23] B. B. Pollock, C. E. Clayton, J. E. Ralph, F. Albert, A. Davidson, L. Divol, C. Filip, S. H. Glenzer, K. Herpoldt, W. Lu, K. A. Marsh, J. Meinecke, W. B. Mori, A. Pak, T. C. Rensink, J. S. Ross, J. Shaw, G. R. Tynan, C. Joshi, and D. H. Froula, Demonstration of a narrow energy spread, ~0.5 GeV electron beam from a two-stage laser wakefield accelerator, Phys. Rev. Lett. **107**, 045001 (2011).

[24] J. S. Liu, C. Q. Xia, W. T. Wang, H. Y. Lu, C. Wang, A. H. Deng, W. T. Li, H. Zhang, X. Y. Liang, Y. X. Leng, X. M. Lu, C. Wang, J. Z. Wang, K. Nakajima, R. X. Li, and Z. Z. Xu, All-optical cascaded laser wakefield accelerator using ionization-induced injection, Phys. Rev. Lett. **107**, 035001 (2011).

[25] M. Chen, E. Esarey, C. B. Schroeder, C. G. R. Geddes, and W. P. Leemans, Theory of ionization-induced trapping in laser-plasma accelerators, Phys. Plasmas **19**, 033101 (2012).

[26] M. Zeng, M. Chen, Z.-M. Sheng, W. B. Mori, and J. Zhang, Self-truncated ionization injection and consequent monoenergetic electron bunches in laser wakefield acceleration, Phys. Plasmas **21**, 030701 (2014).

[27] M. Zeng, M. Chen, L. L. Yu, W. B. Mori, Z. M. Sheng, B. Hidding, D. A. Jaroszynski, and J. Zhang, Multichromatic narrow-energy-spread electron bunches from laser-wakefield acceleration with dual-color lasers, Phys. Rev. Lett. **114**, 084801 (2015).

[28] M. Mirzaie, S. Li, M. Zeng, N. A. M. Hafz, M. Chen, G. Y. Li, Q. J. Zhu, H. Liao, T. Sokollik, F. Liu, Y. Y. Ma, L. M. Chen, Z. M. Sheng, and J. Zhang, Demonstration of self-truncated ionization injection for GeV electron beams, Sci. Rep., **5**, 14659 (2015).

[29] J. P. Couperus, R. Pausch, A. Köhler, O. Zarini, J. M. Krämer, M. Garten, A. Huebl, R. Gebhardt, U. Helbig, S. Bock, K. Zeil, A. Debus, M. Bussmann, U. Schramm, and A. Irman, Demonstration of a beam loaded nanocoulomb-class laser wakefield accelerator, Nat. Commun. **8**, 487 (2017).

[30] M. Kirchen, S. Jalas, P. Messner, P. Winkler, T. Eichner, L. Hübner, T. Hülsenbusch, L. Jeppe, T. Parikh, M. Schnepp, and A. R. Maier, Optimal beam loading in a laser-plasma accelerator, Phys. Rev. Lett. **126**, 174801 (2021).

[31] D. Umstadter, J. K. Kim, and E. Dodd, Laser injection of ultrashort electron pulses into wakefield plasma waves, Phys. Rev. Lett. **76**, 2073 (1996).

[32] G. Fubiani, E. Esarey, C. B. Schroeder, and W. P. Leemans, Beat wave injection of electrons into plasma waves using two interfering laser pulses, Phys. Rev. E **70**, 016402 (2004).

[33] X. Davoine, E. Lefebvre, C. Rechatin, J. Faure, and V. Malka, Cold optical injection producing monoenergetic, multi-GeV electron bunches, Phys. Rev. Lett. **102**, 065001 (2009).

[34] G. Golovin, W. Yan, J. Luo, C. Fruhling, D. Haden, B. Zhao, C. Liu, M. Chen, S. Chen, P. Zhang, S. Banerjee, and D. Umstadter, Electron trapping from interactions between laser-driven relativistic plasma waves, Phys. Rev. Lett. **121**, 104801 (2018).

[35] J. Wang, M. Zeng, X. Wang, D. Li, and J. Gao, Scissor-cross ionization injection in laser wakefield accelerators, Plasma Phys. Controlled Fusion **64**, 045012 (2022).

[36] K. Weichman, K. Miller, B. Malaca, W. Mori, J. Pierce, D. Ramsey, J. Vieira, M. Vranic, and J. Palastro, Analytic pulse technique for computational electromagnetics, Comput. Phys. Commun. **298**, 109096 (2024).

[37] A. Lifschitz, X. Davoine, E. Lefebvre, J. Faure, C. Rechatin, and V. Malka, Particle-in-cell modelling of laser-plasma interaction using fourier decomposition, J. Comput. Phys. **228**, 1803 (2009).

[38] A. Davidson, A. Tableman, W. An, F. Tsung, W. Lu, J. Vieira, R. Fonseca, L. Silva, and W. Mori, Implementation of a hybrid particle code with a PIC description in r-z and a gridless description in ϕ into OSIRIS, J. Comput. Phys. **281**, 1063 (2015).

[39] I. A. Andriyash, R. Lehe, and A. Lifschitz, Laser-plasma interactions with a Fourier-bessel particle-in-cell method, Phys. Plasmas **23**, 033110 (2016).

[40] R. Lehe, M. Kirchen, I. A. Andriyash, B. B. Godfrey, and J.-L. Vay, A spectral, quasi-cylindrical and dispersion-free particle-in-cell algorithm, Comput. Phys. Commun. **203**, 66 (2016).

[41] J.-L. Vay, *Private communication, ALEGRO (Advanced LinEar Collider Study GROup) 2023 Workshop* (DESY, Hamburg, Germany, 2023).

[42] The document of FBPIC for the external fields, https://fbpic.github.io/api_reference/lpa_utilities/external_fields.html.

[43] I. Haber, R. Lee, H. Klein, and J. Boris, Advances in electromagnetic simulation techniques, in *Proceedings of the Sixth Conference on Numerical Simulation of Plasmas, Berkeley, CA* (1973), pp. 46–48.

[44] J.-L. Vay, I. Haber, and B. B. Godfrey, A domain decomposition method for pseudo-spectral electromagnetic simulations of plasmas, J. Comput. Phys. **243**, 260 (2013).

[45] L. Fedeli, A. Huebl, F. Boillod-Cerneux, T. Clark, K. Gott, C. Hillairet, S. Jaure, A. Leblanc, R. Lehe, A. Myers, C. Piechurski, M. Sato, N. Zaim, W. Zhang, J.-L. Vay, and H. Vincenti, Pushing the frontier in the design of laser-based electron accelerators with groundbreaking mesh-refined particle-in-cell simulations on exascale-class supercomputers, in *Proceedings of the International Conference for High Performance Computing, Networking, Storage and Analysis (SC22)* (IEEE, New York, 2022), pp. 1–12.

[46] R. Lehe, M. Kirchen, I. A. Andriyash, B. B. Godfrey, and J.-L. Vay, A spectral, quasi-cylindrical and dispersion-free particle-in-cell algorithm, Comput. Phys. Commun. **203**, 66 (2016).

[47] J.-L. Vay *et al.*, Modeling of a chain of three plasma accelerator stages with the WarpX electromagnetic PIC code on GPUs, Phys. Plasmas **28**, 023105 (2021).

[48] M. Zeng, A. Martinez de la Ossa, K. Poder, and J. Osterhoff, Plasma eyepieces for petawatt class lasers, Phys. Plasmas **27**, 023109 (2020).

[49] M. Zeng, A. M. de la Ossa, and J. Osterhoff, Ponderomotively assisted ionization injection in plasma wakefield accelerators, New J. Phys. **22**, 123003 (2020).

[50] B. M. Cowan, D. L. Bruhwiler, J. R. Cary, E. Cormier-Michel, and C. G. R. Geddes, Generalized algorithm for control of numerical dispersion in explicit time-domain electromagnetic simulations, Phys. Rev. ST Accel. Beams **16**, 041303 (2013).

[51] P. Mora and T. M. Antonsen, Kinetic modeling of intense, short laser pulses propagating in tenuous plasmas, Phys. Plasmas **4**, 217 (1997).

[52] M. Zeng, The GIT repository for a tracking code of particles scattered by single or multiple lasers, with both

first-principle and ponderomotive force algorithms (2022), https://github.com/mingzeng8/ponderomotive_scatter.

[53] Z.-M. Sheng, K. Mima, Y. Sentoku, M. S. Jovanović, T. Taguchi, J. Zhang, and J. Meyer-ter Vehn, Stochastic heating and acceleration of electrons in colliding laser fields in plasma, Phys. Rev. Lett. **88**, 055004 (2002).

[54] Z.-M. Sheng, K. Mima, J. Zhang, and J. Meyer-ter Vehn, Efficient acceleration of electrons with counterpropagating intense laser pulses in vacuum and underdense plasma, Phys. Rev. E **69**, 016407 (2004).

[55] See Supplemental Material at http://link.aps.org/supplemental/10.1103/PhysRevAccelBeams.28.021301 for the snapshots of the acceleration process for the case $\theta = 20°$.

[56] B. Hidding *et al.*, Progress in hybrid plasma wakefield acceleration, Photonics **10**, 99 (2023).

[57] The GIT repository for the PIC code WarpX, https://github.com/ECP-WarpX/WarpX.